

## Article

# Thin 1,2,4-Triazole Films for the Inhibition of Carbon Steel Corrosion in Sulfuric Acid Solution

Yaroslav G. Avdeev <sup>\*</sup>, Tatyana A. Nenasheva, Andrey Yu. Luchkin <sup>\*</sup>, Andrey I. Marshakov <sup>\*</sup> and Yurii I. Kuznetsov <sup>\*</sup>

A.N. Frumkin Institute of Physical Chemistry and Electrochemistry, Russian Academy of Sciences, Moscow 119071, Russia; nenasheva@ipc.rssi.ru

<sup>\*</sup> Correspondence: avdeevavdeev@mail.ru (Y.G.A.); andreylichkin23@gmail.com (A.Y.L.); mar@ipc.rssi.ru (A.I.M.); yukuzn@gmail.com (Y.I.K.)

**Abstract:** Etching of steel items in sulfuric acid solution is used in various human activities (oil and gas industry, metal production, utilities, transport, etc.). This operation is associated with significant material costs due to corrosion losses of the metal. It has been found that an efficient way to prevent corrosion of steel in sulfuric acid solution involves the formation of thin protective films consisting of corrosion inhibitor molecules of triazole class on its surface. It has been shown that the protection of steels with a 3-substituted 1,2,4-triazole (3ST) in H<sub>2</sub>SO<sub>4</sub> solution is accompanied by the formation of a polymolecular layer up to 4 nm thick. The 3ST layer immediately adjacent to the steel surface is chemisorbed on it. The efficiency of this compound as an inhibitor of corrosion and hydrogen absorption by steel is determined by its ability to form a protective organic layer, as experimentally confirmed by XPS and AFM data. The kinetic constants of the main stages of hydrogen evolution and permeation into steel in the H<sub>2</sub>SO<sub>4</sub> solution were determined. A significant decrease in both the reaction rate of cathodic hydrogen evolution and the rate of hydrogen permeation into steel by the triazole in question was noted. It has been shown that the preservation of the metal plasticity in the acid medium containing the triazole under study is due to a decrease in the hydrogen concentration in the metal bulk.

**Keywords:** thin films; 1,2,4-triazole; acid corrosion; corrosion inhibition; hydrogen permeation into the metal; carbon steel; sulfuric acid solution



**Citation:** Avdeev, Y.G.; Nenasheva, T.A.; Luchkin, A.Y.; Marshakov, A.I.; Kuznetsov, Y.I. Thin 1,2,4-Triazole Films for the Inhibition of Carbon Steel Corrosion in Sulfuric Acid Solution. *Coatings* **2023**, *13*, 1221. <https://doi.org/10.3390/coatings13071221>

Academic Editor: Mingwen Bai

Received: 6 June 2023

Revised: 1 July 2023

Accepted: 5 July 2023

Published: 7 July 2023



**Copyright:** © 2023 by the authors. Licensee MDPI, Basel, Switzerland. This article is an open access article distributed under the terms and conditions of the Creative Commons Attribution (CC BY) license (<https://creativecommons.org/licenses/by/4.0/>).

## 1. Introduction

The formation of thin protective films on the surfaces of metals and alloys is an efficient method for preventing their corrosion in corrosive media [1–5]. Thin films on metal surfaces can be formed by molecules of organic inhibitors added to the corrosive environment. This method of inhibitor protection of metals makes it possible to hinder the corrosion in solutions of mineral acids that are the most corrosive aqueous media. Upon addition of unsaturated organic compounds (acetylated alcohols [6–13] or unsaturated aldehydes [14–17]) to solutions of acids, polymeric films are formed on metal surfaces. In this case, an unsaturated organic compound acts as a monomer that is converted to an organic polymer on the steel surface, thus blocking the metal surface from contact with the corrosive environment. Organic polymeric films formed from unsaturated organic compounds can protect steel structures from hydrochloric acid at temperatures above 100 °C [18]. The protective 1,2,4-triazoles films formed on steels in inhibited mineral acid solutions are less studied. It is important to estimate the potential of this steel protection method in sulfuric acid solutions. Sulfuric acid solutions are widely and successfully used in various industries—for example, in metallurgy to remove thermal scale, rust, and mineral deposits from steel items [19–22].

The results obtained in studies on the properties of 1,2,4-triazole surface films are important for expanding our theoretical understanding in the field of metal corrosion inhibition.

Upon contact with acid solutions, steel items not only undergo general corrosion but also lose mechanical ductility due to hydrogen absorption by the metal. The ductility of steel is often affected by hydrogen embedded in the metal bulk [23–28].

Unfortunately, though the known organic corrosion inhibitors (CIs) slow down general corrosion of steel well enough, they have almost no effect on the preservation of its strength since they poorly prevent hydrogen absorption by it. Only some nitrogen-containing organic CIs were observed to reduce the rate of hydrogen permeation into steel in acid environments [29,30].

In view of this, it seems important to identify the effect of thin triazole films on the general corrosion of steel, on the process of hydrogen absorption by this material, and on how the metal maintains its mechanical properties.

In this study, a 3-substituted 1,2,4-triazole (3ST, [(C<sub>6</sub>H<sub>5</sub>CH<sub>2</sub>)<sub>3</sub>N–C<sub>2</sub>H<sub>2</sub>N<sub>3</sub>]Cl) that belongs to the promising class of triazole compounds [31–34] was chosen as the CI. The choice of this compound is due to its potential ability to form thin protective films characteristic of triazoles on metals. Earlier [28], we conducted a study of the action of 3ST on the corrosion and strength properties of steels in aggressive environment. It was found that the maximum effect was observed in the presence of 5 mM inhibitor in the solution.

## 2. Materials and Methods

Samples of spring steel (composition, mass: 0.65%–0.75% carbon, 1.4%–1.7% silicon, 0.4%–0.6 % manganese and 0.2%–0.4% chromium) and carbon steel (composition, mass: 0.05%–0.11% carbon, up to 0.03% silicon, 0.25%–0.50% manganese, up to 0.25% nickel, up to 0.04% sulfur, up to 0.035% phosphorus, up to 0.01% chromium, and up to 0.25% copper) were used as the working electrodes. Spring steel is most prone to hydrogen embrittlement, so the effect of hydrogen concentration on the mechanical properties (ductility) of the metal was studied on samples of this steel.

Before starting each experiment, the surface of the steel surface was ground on abrasive wheels of different grit sizes, polished with ASM 0.5/0—abrasive and cleaned with dimethyl ketone.

An aqueous 2 M solution of sulfuric acid was used as a reference medium for testing studies. It was prepared from the concentrated acid of “chemically pure” grade and distilled water. The solutions used in the electrochemical studies were deaerated with argon. Corrosion tests were carried out in freely aerated solutions. The 3ST derivative was studied as the CI.

### 2.1. Methods

#### 2.1.1. Gravimetric Method

The corrosion rate of spring steel was determined from the mass loss of samples (83.5 mm × 10 mm × 0.5 mm) with an area of 17.6 cm<sup>2</sup> in 2 M H<sub>2</sub>SO<sub>4</sub> solution.

$$\rho = \Delta m S^{-1} \tau^{-1} \quad (1)$$

where  $\Delta m$  is the mass change of the steel coupons,  $S$  is the sample area, and  $\tau$  is the duration of the corrosion test.

The CI efficiency was estimated as the inhibition coefficient:

$$Z = (\rho_0 - \rho_{\text{inh}}) \rho_0^{-1} 100\% \quad (2)$$

where  $\rho_0$  and  $\rho_{\text{inh}}$  are steel coupon corrosion rates in an aggressive environment in the absence and presence of CI.

#### 2.1.2. Atomic Force Microscopy (AFM) Method

After keeping the samples in the corrosive environment, their topography was estimated using an atomic force microscope (SolverNext II made by NovaFotonix, Moscow, Russia). A silicon probe (resonance frequency 273 kHz, elasticity coefficient 4.5 N/m) was used.

### 2.1.3. Determination of the Amount of Hydrogen Absorbed by the Metal by Means of Vacuum Extraction

The amount of hydrogen absorbed by spring steel was determined by vacuum extraction. A steel coupon kept in an acid solution was placed in a quartz chamber. The air was pumped out of the chamber. The temperature of the chamber was increased to 500 °C. The amount of hydrogen released from the steel coupon was determined from the increase in pressure measured with a mercury manometer. The pressure of released hydrogen ( $P_{H_2}$ ) was calculated by the formula

$$P_{H_2} = P_{total} - P_{base} \quad (3)$$

where  $P_{base}$  is the base pressure (0.3 kPa) determined by the tightness of the experimental installation.

The hydrogen concentration in the steel bulk ( $\text{mol} \cdot \text{cm}^{-3}$ ) was calculated by the formula

$$C_H^v = K P_{H_2} V^{-1} \quad (4)$$

where  $K$  is a parameter determined by the internal volume of the installation, and  $V$  is the volume of the steel coupon.

The decrease in the hydrogen concentration in the steel bulk was determined by the formula

$$Z_H^v = \frac{C_H^v - C_{H,inh}^v}{C_H^v} 100\% \quad (5)$$

where  $C_H^s$  and  $C_{H,inh}^v$  are molar concentration of hydrogen in the volume of the metal after holding in an aggressive environment in the absence and presence of CI, respectively.

### 2.1.4. Determination of Mechanical Properties (Ductility) of Steel

The ductility of spring steel ( $\pi$ ) was determined as the ratio of the number of bends after exposure to the corrosive environment ( $\beta$ ) and before fracture of specimens in the initial state ( $\beta_0$ ):

$$\pi = \frac{\beta}{\beta_0} 100\% \quad (6)$$

The mean number of bends until the fracture of samples in the initial state was 87.

### 2.1.5. Voltammetric Studies

The voltammetric curves of spring steel samples were obtained in deaerated stirred 2 M  $\text{H}_2\text{SO}_4$  solutions using a potentiostat at a potential scanning rate of  $0.5 \text{ mV} \cdot \text{s}^{-1}$  after exposure for 30 min to the solution being studied. The effect of the CI on the kinetics of electrode reactions was characterized using the coefficient

$$\gamma = i_{a,0} (i_{a,inh})^{-1} \quad (7)$$

where  $i_{a,0}$  and  $i_{a,inh}$  are the steel electrode current density in an aggressive environment in the absence and presence of CI.

### 2.1.6. Permeation Test

The kinetics of permeation of hydrogen formed at the cathode into the metal were studied in a two-compartment glass electrochemical cell (Figure 1) [35,36]. The working electrode was a carbon steel membrane with a thickness of 100  $\mu\text{m}$  and a working area of 4.25  $\text{cm}^2$ .

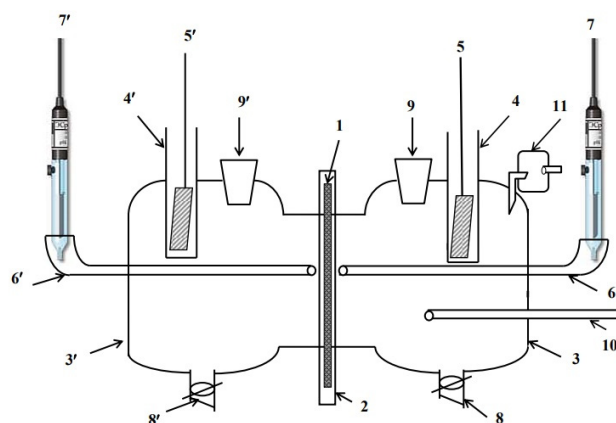


**Figure 1.** Devanatkhan–Stakhursky electrochemical cell. 1—working electrode (membrane); 2—Teflon holder; 3—working part of the cell; 3'—diffusion part of the cell; 4, 4'—auxiliary electrode cell; 5, 5'—auxiliary electrode; 6, 6'—electrolytic switch; 7, 7'—reference electrode; 8, 8'—tap for draining the solution; 9, 9'—solution feed into the cell.

The working side of the membrane was cathodically polarized. The stationary current of hydrogen penetration through the membrane ( $i_p$ ) was recorded on the anodically polarized (diffusion) side of the membrane. The diffusion part of the cell was filled with 0.1 M NaOH, and the membrane was polarized at a potential of 0.45 V vs. SHE. To facilitate the hydrogen ionization process, a layer of palladium was deposited onto the diffusion side of the membrane (Figure 1). The procedures of membrane preparation and performing the experiment were reported elsewhere [28].

#### 2.1.7. Electrochemical Impedance Spectroscopy (EIS)

The adsorption of the CI was studied by EIS on a rotating (1000 rpm) carbon steel disk (0.64 cm<sup>2</sup>). The cathode potential of the steel was kept constant ( $E = -0.30$  V). The measurements were carried out in a glass cell with a separate space for the counter and reference electrodes. The steel was kept in the acid solution until repetitive similar impedance spectra were established (2 h). After that, 3ST was added, and the metal was kept until a steady-state view of the spectrum was achieved (no longer than 3 h).

The surface coverage with the CI ( $\theta_{inh}$ ) was determined using the formula

$$\theta_{inh} = \frac{C_{dl}^0 - C_{dl}}{C_{dl}^0 - C_{dl,max}} \quad (8)$$

where  $C_{dl}^0$ ,  $C_{dl}$ , and  $C_{dl,max}$  are the capacitances of the electrode in the background solution, in the inhibited solution, and in the inhibited solution where the maximum CI adsorption on the metal is achieved, respectively.

#### 2.1.8. XPS Studies of Steel Surface

The surface layers formed by the CI on the steel surface were studied by X-ray photoelectron spectroscopy (XPS) using an HB100 Auger microscope (VG, UK) equipped with an additional chamber for getting XPS spectra. The vacuum in the analytical chamber was no worse than 10<sup>-9</sup> Torr. An aluminum anode (power 200 W) was used as the excitation source; the pass energy of the analyzer was 50 eV. Steel disks with a diameter of 10 mm were used as the samples.

The binding energy ( $E_b$ ) of electrons knocked out from the inner shells of the atoms was calibrated by the XPS peak of C1s electrons (285.0 eV) from the deposited vapors of the diffusion pump oil. The spectrometer was calibrated vs. the binding energies of copper and gold samples: Cu2p<sub>3/2</sub> = 932.7 and Au4f<sub>7/2</sub> = 84.0 eV. The peaks of the following elements were studied: C1s, O1s, Fe2p, N1s, and S2p. The quantitative estimation of the photoionization cross sections of the corresponding electron shells was performed similarly to

that reported elsewhere [37]. The integral intensities of peaks were calculated by the Shirley method [38]. The peak position was determined with an accuracy of  $\pm 0.1$  eV. The element ratios were calculated using the integral intensities under the peaks, taking into account the photoionization cross sections  $\sigma$  of the corresponding electron shells, with the introduced corrections, which were obtained from the analysis of compounds with known stoichiometry.

In some cases, prolonged ultrasonic cleaning (up to 18 min) of metal samples by distilled water was carried out. During such cleaning, the physisorbed CI is removed from the surface of the steel. The chemisorbed CI molecules were not removed during ultrasonic washing of the metal surface [39].

### 2.1.9. Studies on the Protective Aftereffect of Thin Films of 3ST on Steel

The protective aftereffect of 3ST films was studied by the gravimetric method in 2 M  $\text{H}_2\text{SO}_4$ . Samples of carbon steel with a thickness of 2 mm and a working area of 30  $\text{cm}^2$  were used in the experiments. The samples were placed for 2–96 h into 2 M  $\text{H}_2\text{SO}_4$  containing 5 mM of 3ST. After that, some of the samples were abundantly washed with distilled water and transferred to the uninhibited acid solution. The remaining samples were used to determine the mass loss of the metal in the inhibited acid solution (see Section 2.1.1). Calculations of the inhibitor's protective aftereffect were made with correction for the corrosion loss of the metal in the inhibited acid solution.

In all the experiments, platinum counter electrodes and silver chloride reference electrodes were used. The electrode potentials are given vs. standard hydrogen electrode (SHE).

Electrochemical measurements were performed using IPC potentiostat (Kronas LLC, Moscow, Russia).

The experimental data presented in the manuscript were obtained at  $25 \pm 1$  °C.

## 3. Results and Discussion

### 3.1. Effect of the Inhibitor on the Corrosion and Mechanical Properties of Steel

The decrease in the rate of hydrogen permeation into a metal in the presence of CIs is traditionally studied on spring steels that are most susceptible to hydrogen absorption by the metal bulk. In 2 M  $\text{H}_2\text{SO}_4$  solution, addition of 5 mM of 3ST reduces the corrosion rate of steel  $\rho$  and the hydrogen concentration in the metal bulk  $C_H^s$  (Table 1). In 2 M  $\text{H}_2\text{SO}_4$  solution that is extremely corrosive to the steel, the plastic properties of the latter ( $\pi$ ) in the presence of the CI are partially preserved (Table 1). Hence, 3ST inhibits the general corrosion of steel and reduces hydrogen permeation into the metal.

**Table 1.** Effect of 5 mM 3ST on the corrosion rate of spring steel in 2 M  $\text{H}_2\text{SO}_4$ , hydrogen concentration in steel, and steel ductility.

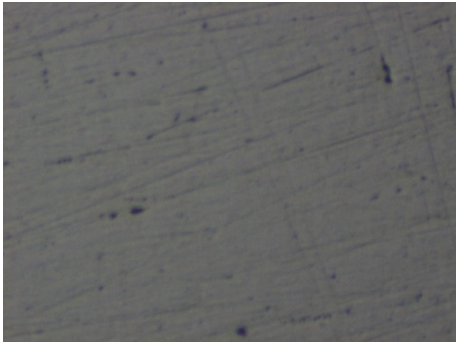
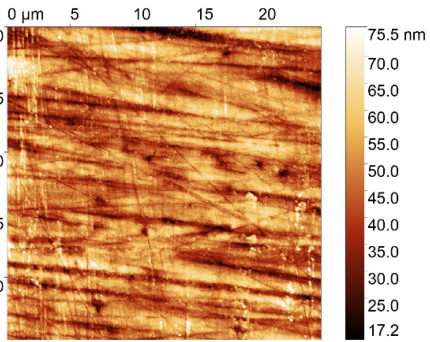
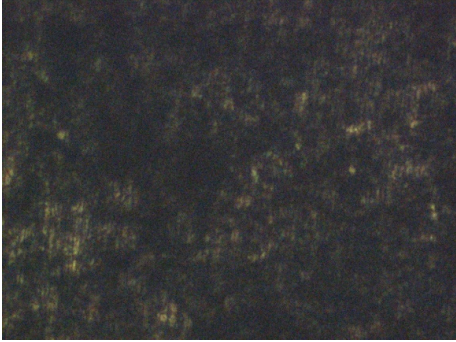
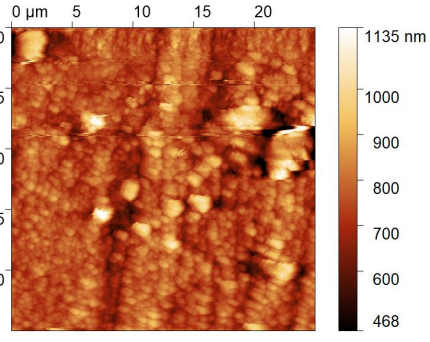
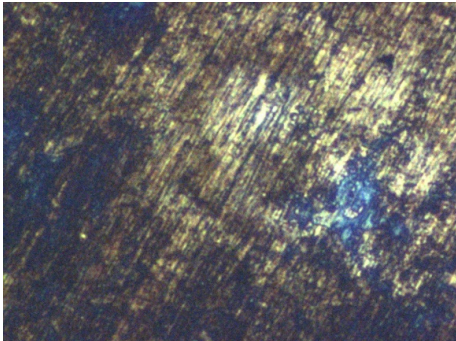
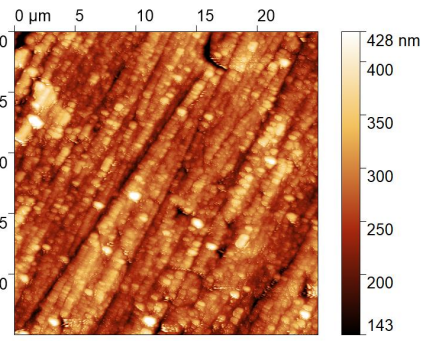
| Solution   | $\rho$ , $\text{g m}^{-2} \cdot \text{h}^{-1}$ | $Z_{\text{cor}}$ , % | $C_H^v$ , $\text{mol cm}^{-3}$ | $Z_H^v$ *, % | $\pi$ , % |
|------------|--|----------------------|--------------------------------|--------------|-----------|
| Background | 35.3   | -                    | $1.92 \times 10^{-5}$          | -            | -*        |
| CI         | 0.71   | 98.0                 | $4.20 \times 10^{-7}$          | 97.8         | 32        |

\* total loss of ductility.

### 3.2. Effect of the CI on the State of Steel Surface

Table 2 presents the microphotographs and AFM images of the steel surface taken before and after etching in the  $\text{H}_2\text{SO}_4$  solution.

**Table 2.** Microphotographs of steel surface after exposure to 2 M H<sub>2</sub>SO<sub>4</sub> solution (2 h).

| No. | Treatment                                   | Microphotographs<br>(400 × 600 μm)   | AFM Images<br>(25 × 25 μm)  |
|-----|---|--|---|
| 1   | None  |    |    |
| 2   | 2 M H <sub>2</sub> SO <sub>4</sub>          |   |   |
| 3   | 2 M H <sub>2</sub> SO <sub>4</sub> + 5mM CI |  |  |

The microphotograph of the steel sample that did not undergo etching clearly shows traces of polishing such as scratches and surface undulations. The AFM image also showed the presence of surface scratches up to 0.03 μm deep. The mean surface roughness was  $0.05 \pm 0.01$  μm. After etching a sample in 2 M H<sub>2</sub>SO<sub>4</sub>, a sludge layer was observed on the surface, while the number of scratches decreased significantly due to steel etching. The AFM image shows surface structures up to 5 μm in diameter and up to 1.2 μm high. The mean roughness after etching increased almost 15-fold to reach  $0.75 \pm 0.08$  μm.

The addition of 3ST to the aggressive environment improves the quality of the steel surface. The average surface roughness is significantly smaller compared to the background solution and amounts to  $0.27 \pm 0.04$  μm.

### 3.3. Effect of the CI on the Rates of Electrode Reactions on Steel

The presence of the CI in 2M H<sub>2</sub>SO<sub>4</sub> solution slows down both the cathodic and anodic reaction rates on spring steel (Figure 2). The addition of 5 mM of the 3ST decreases the rates of anodic and cathodic reactions at  $E = -0.10$  V and  $-0.30$  V by a factor of 130 and 6, respectively. The values of the corrosion potential in the background solution and in

the presence of 3ST are  $-0.23\text{ V}$  and  $-0.12\text{ V}$ , respectively. Consequently, 3ST inhibits and predominantly slows down the anodic reaction of the steel.

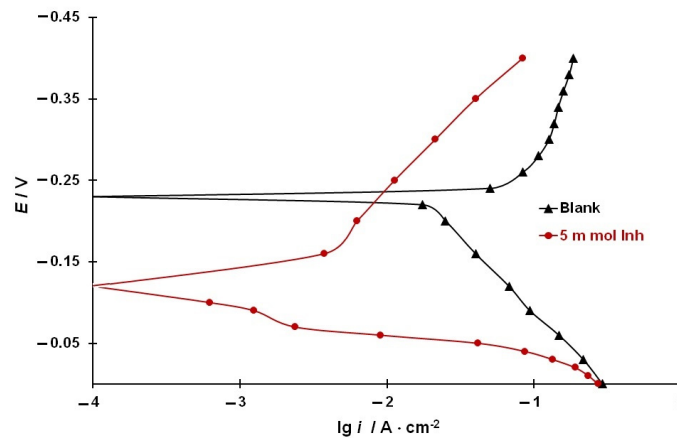


**Figure 2.** Current–voltage curves on spring steel in 2 M H<sub>2</sub>SO<sub>4</sub> without and in the presence of 5 mM 3ST.

### 3.4. Kinetics of Hydrogen Evolution and Permeation into the Metal

The cathodic curves and the plots of the rate of hydrogen permeation into steel on potential in sulfuric acid solution and with addition of 5 mM 3ST are shown in Figure 3. The inhibitor abruptly decreases the rates of hydrogen evolution ( $i_c$ ) and permeation into steel ( $i_p$ ).

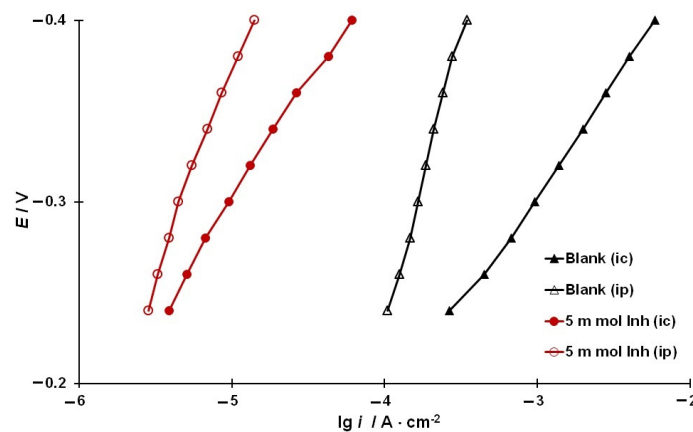


**Figure 3.** Cathodic curves and plots of the rate of hydrogen permeation into steel vs. potential.

### 3.5. Rate Constants of the Main Stages of Hydrogen Evolution and Permeation into Steel

The cathodic curves and the plots of the permeation current on potential in sulfuric acid solution and with addition of 5 mM 3ST are shown in Figure 3. The inhibitor abruptly decreases the rates of hydrogen evolution ( $i_c$ ) and permeation into steel ( $i_p$ ).

The basics of IPZ [40] analysis for calculating the rate constants of the main stages of cathodic evolution and hydrogen absorption by a metal in an acid solution containing an organic inhibitor are given in [28]. Therefore, we will only give the equations required for the calculation of these constants along with their brief description.

It is assumed that the discharge of H<sup>+</sup> ions occurs on the steel surface unoccupied by adsorbed H atoms and inhibitor particles. Then, the rate of this reaction ( $i_c$ ) is described as [40–42]

$$i_c = Fk_c\alpha_{H^+} \left[ (1 - \theta_{inh})^{r_1} - \theta_H \right] \exp(-\alpha FE/RT) \tag{9}$$

where  $k_c$  is the rate constant of discharge of hydrogen ions;  $\alpha_{H^+}$  is the activity of hydrogen ions;  $\theta_{inh}$  is the coverage of the electrode surface with inhibitor particles;  $r_1$  is the number of adsorption sites that a hydrogen ion occupies on the surface;  $\theta_H$  is the surface coverage

of the electrode with hydrogen;  $\alpha$  is the transfer coefficient of the hydrogen ion discharge reaction;  $F$  is the Faraday constant;  $R$  is the gas constant; and  $T$  is the absolute temperature.

If the reaction of recombination of H atoms is irreversible [40,41], its rate ( $i_r$ ) is defined as

$$i_r = Fk_r\theta_H^2 \quad (10)$$

where  $k_r$  is the rate constant.

The rate of hydrogen transfer through the surface ( $i_p$ ) and its steady-state diffusion in the membrane are described as

$$i_p = F(k_{abs}\theta_H - k_{des}C_H^s) \quad (11)$$

and

$$i_p = \frac{FDC_H^s}{L} \quad (12)$$

where  $k_{abs}$  and  $k_{des}$  are the rate constants of the interface reactions;  $C_H^s$  is the surface concentration of diffusible hydrogen in the metal (subsurface concentration);  $L$  is the membrane thickness; and  $D$  is the diffusion coefficient of hydrogen in the metal.

It follows from Equations (11) and (12) that

$$\theta_H = \frac{k_{des} + \frac{D}{L}}{k_{abs}} C_H^s = kC_H^s \quad (13)$$

where  $k$  is the kinetic-diffusion constant [40].

Using Equations (9), (10), (12), and (13), we can obtain for steady-state conditions ( $i_c = i_p + i_r$ ) [28,40,43]:

$$i_c \exp\left(\frac{\alpha FE}{RT}\right) = Fk_1 a_{H^+} (1 - \theta_{inh})^{r1} - \frac{k_1 a_{H^+} kL}{D} \cdot i_p \quad (14)$$

$$i_p = \frac{D\sqrt{F}}{Lk\sqrt{k_r}} \cdot \sqrt{i_c - i_p} = \frac{D\sqrt{F}}{Lk\sqrt{k_r}} \sqrt{i_r} \quad (15)$$

By combining Equations (9), (10), (12), and (13), we can calculate the hydrogen surface coverage

$$\theta_H = \frac{-\left(k_{1,i} + \frac{D}{Lk}\right) + \sqrt{\left(k_{1,i} + \frac{D}{Lk}\right)^2 + 4k_r k_{1,i} (1 - \theta_{inh})^{r1}}}{2k_r} \quad (16)$$

where  $k_{1,i} = k_1 a_{H^+} \cdot \exp\left(\frac{\alpha FE_i}{RT}\right)$  is the formal rate constant of cathodic reaction at the  $E_i$  potential. The subsurface concentration of diffusible hydrogen ( $C_H^s$ ) can be calculated from  $i_p$  values using Equation (12) or from  $\theta_H$  values using Equation (13).

The cathodic curves and the plots of the permeation current vs. potential obtained without and in the presence of the CI are shown in Figure 3. In accordance with Equation (15), the plots of  $i_p$  vs.  $i_r^{0.5}$  should be linear and should pass through the origin. Figure 4 shows the plots of  $i_p$  vs.  $i_r^{0.5}$  obtained both in the background solution and in the solution containing 5 mM CI. The transfer coefficients  $\alpha$  were calculated by comparing the  $\frac{dE}{d \log i_c}$  and  $\frac{dE}{d \log i_p}$  values (Figure 2) and using the IPZ method [40]. Then, the values of the  $f = i_c \exp(\alpha FE/RT)$  function were calculated, and the graphs of  $f$  vs.  $i_p$  were plotted (Figure 5).

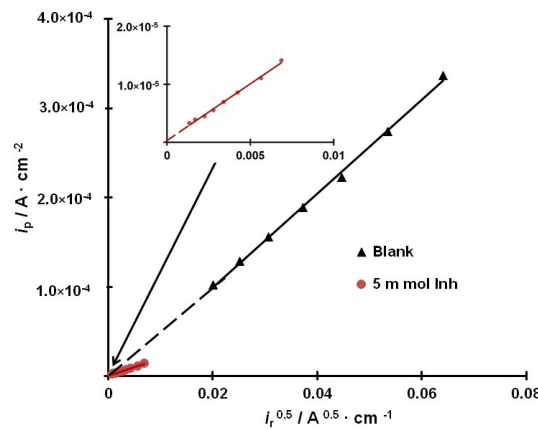


**Figure 4.** Plot of the permeation current vs. the rate of hydrogen chemical recombination in 2 M H<sub>2</sub>SO<sub>4</sub> containing 5 mM 3ST.

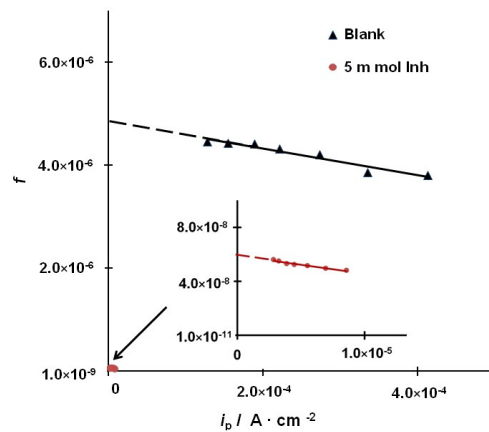


**Figure 5.** Plot of the  $f = i_c \exp(\alpha FE/RT)$  function vs. the permeation current in 2 M H<sub>2</sub>SO<sub>4</sub> containing 5 mM 3ST.

To calculate the  $k_1$ ,  $k_r$ , and  $k$  constants by Equations (14) and (15), the  $\theta_{inh}$  value is required. In solutions containing the CI, the inhibitor surface coverage was determined by the EIS method. The characteristic impedance spectra in the background and inhibited H<sub>2</sub>SO<sub>4</sub> solutions presented as Nyquist plots are ideal half-circles that can be fitted using a simple equivalent circuit that comprises the double electric layer capacitance ( $C_{dl}$ ), charge transfer resistance ( $R_{ct}$ ), and solution resistance ( $R_s$ ) (Figure 6).

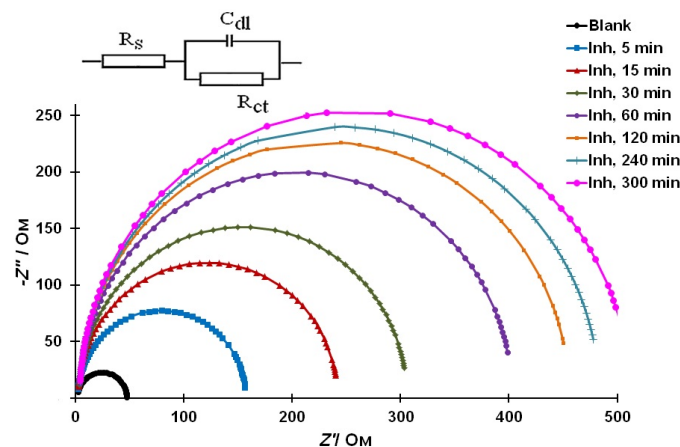


**Figure 6.** Nyquist plots of steel in 2 M H<sub>2</sub>SO<sub>4</sub> recorded after adding 0.05 mM 3ST to the aggressive environment after various exposure times.

It is shown that an increase in the residence time of steel in an inhibited medium is accompanied by an increase in the hodograph diameter. This is characteristic of a slow adsorption process. The plot of the steady-state values of  $\theta_{\text{inh}}$  calculated by Equation (8) on the inhibitor concentration in the solution is shown in Figure 7. At a concentration of 5 mM 3ST, the inhibitor surface coverage was 0.99; this value was used in the subsequent calculations.

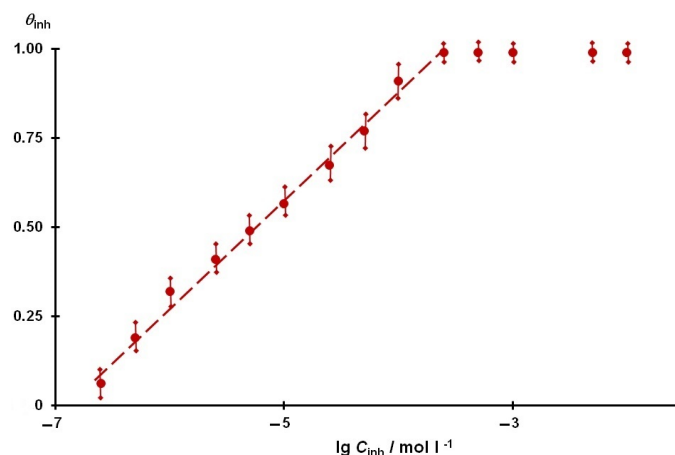


Figure 7. Adsorption isotherm of 3ST on carbon steel ( $E = -0.30$  V) from 2 M  $\text{H}_2\text{SO}_4$ .

Using the  $\alpha$  and  $\theta_{\text{inh}}$  values (Table 3) and assuming that  $r_1 = 0.3$  [44], the  $k_{c,i}$  and  $k$  values were calculated by Equation (15) from the slope of the  $f, i_p$  lines (Figure 5) and the intercept on the ordinate axis at  $i_p = 0$  (Table 3).

Table 3. Kinetic constants, hydrogen surface coverages ( $\theta_H$ ) and surface concentrations of diffusible hydrogen ( $C_H^s$ ) under cathodic polarization ( $E = -0.3$  V) of steel in 2 M  $\text{H}_2\text{SO}_4$ , solution containing 3ST.

| Additive             | $k_{1,i,r}$<br>$\text{mol cm}^{-2} \text{s}^{-1}$ | $k_r$<br>$\text{cm}^3 \text{mol}^{-1}$ | $k_{r,r}$<br>$\text{mol cm}^{-2} \text{s}^{-1}$ | $\theta_H \times 100$ | $C_H^s$<br>$\text{mol cm}^{-3}$ |
|----------------------|---|--|---|-----------------------|---------------------------------|
| None<br>(background) | $1.14 \times 10^{-8}$                             | $1.50 \times 10^5$                     | $7.05 \times 10^{-6}$                           | 3.65                  | $2.34 \times 10^{-7}$           |
| CI                   | $9.94 \times 10^{-11}$                            | $3.69 \times 10^6$                     | $9.46 \times 10^{-8}$                           | 1.61                  | $6.39 \times 10^{-9}$           |

Based on the slopes of the  $i_p$  vs.  $i_r^{0.5}$  plots (Figure 4) and taking the  $k$  value and the stationary hydrogen diffusion coefficient  $D = 7.3 \times 10^{-5} \text{ cm}^2 \cdot \text{s}^{-1}$  [45] into consideration, the value of  $k_r$  was determined from Equation (14) (Table 3).

The calculated values of the kinetic constants, both in the background solution and in the solution containing 5 mM 3ST, are presented in Table 3.

The values of  $\theta_H$  ( $E = -0.3$  V) in the background 2 M  $\text{H}_2\text{SO}_4$  solution and in the presence of the CI were calculated using Equation (16) (Table 1). Addition of the CI reduces  $\theta_H$  more than twofold.

The subsurface concentration of hydrogen in steel ( $C_H^s$ ) was calculated using Equations (12) and (13). The discrepancy between the values obtained did not exceed 10% (Table 3 shows the mean values of  $C_H^s$ ).

The results obtained are consistent with the data of Section 3.1—that is, the CI decreases both the total hydrogen content ( $C_H^v$ ) in the metal and that of diffusible hydrogen ( $C_H^s$ ).

As we can see, in the presence of the CI in the  $\text{H}_2\text{SO}_4$  solution, the concentration of hydrogen in the metal decreases sharply, which, as shown above in Section 3.1, has a beneficial effect on the mechanical properties of the metal and, hence, favors an increase in its resistance to stress corrosion cracking.

### 3.6. The Adsorption Interaction of the Steel Surface with the Inhibitor

The efficient inhibition of the electrode reactions and hence of steel corrosion by 3ST is probably due to the chemical interaction between the metal surface and the CI molecules. It is important to understand the nature of the CI interaction with the steel. The adsorption of 3ST on the surface of carbon steel obeys the Temkin isotherm:

$$\theta_{inh} = f_n^{-1} \ln[BC_{inh}] \quad (17)$$

where  $f_n$  is the surface heterogeneity factor, and  $B$  is the adsorption equilibrium constant (Figure 7). The calculated  $f_n$  value is 7.56,  $B = 8.74 \cdot 10^6 \text{ L mol}^{-1}$ . The free adsorption energy ( $-\Delta G_{ads}$ ) is calculated according to the equation

$$-\Delta G_{ads} = RT \ln 55.5 B \quad (18)$$

and amounts to  $(-\Delta G_{ads}) = 49 \text{ kJ mol}^{-1}$ .

The high value of  $(-\Delta G_{ads})$  thus obtained is indicative, with high probability, of the chemisorption nature of interaction the metal surface with CI. The chemical bonding of the steel surface with the inhibitor molecules results in the formation of protective surface layers that inhibit corrosion most efficiently.

### 3.7. The Protective Layers Formed by 3ST on the Steel

The protective layers formed on the steel surface are studied using the XPS method. Analysis of the samples coated with a thin film of CI showed the presence of layers with a complex composition on the surface. The position of complex peaks of  $\text{Fe}2p_{3/2}$  XPS spectra of Fe and their satellite peaks (Figure 8) indicates that the steel surface contains a layer consisting of  $\text{Fe}_3\text{O}_4$  ( $E_b = 710.8 \text{ eV}$ ). The presence of different types of O is indicated by the O1s spectrum that can be decomposed into three peaks arising from O in the  $\text{Fe}_3\text{O}_4$  lattice ( $E_b = 530.3 \text{ eV}$ ), hydroxyl groups ( $531.8 \text{ eV}$ ), and adsorbed water molecules ( $533.5 \text{ eV}$ ) (Figure 9).

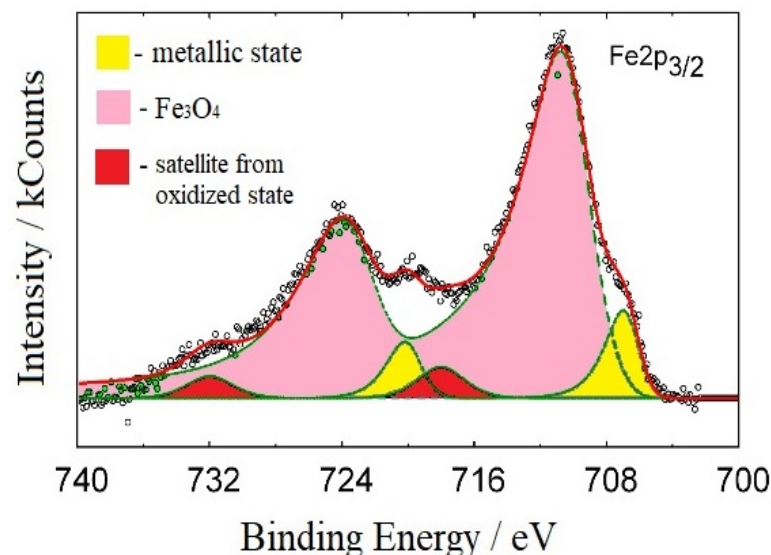


**Figure 8.** XPS spectrum of Fe2p electrons from the surface of carbon steel. Steel coupon processing: 2 M  $\text{H}_2\text{SO}_4$  + 5 mM 3ST, test duration—24 h.

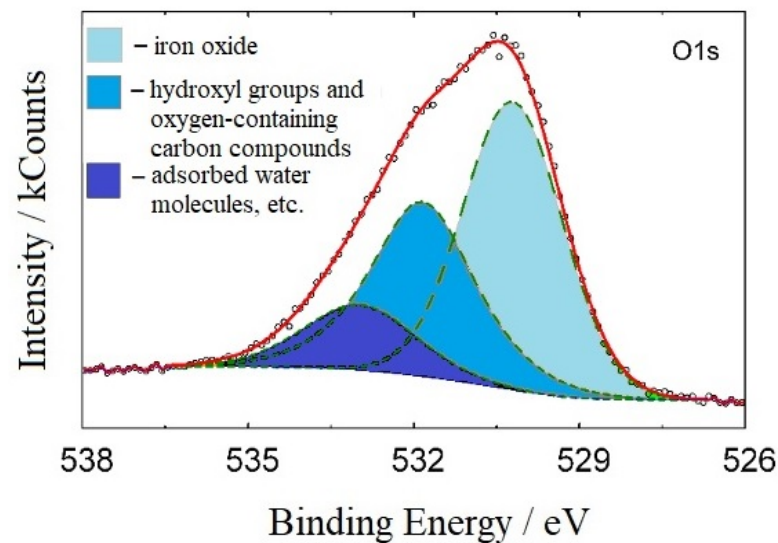


**Figure 9.** XPS spectrum of N1s electrons from the surface of carbon steel. Steel coupon processing: 2 M H<sub>2</sub>SO<sub>4</sub> + 5 mM 3ST, test duration—24 h. Coupon cleaned in ultrasonic bath.

The XPS spectrum of N1s electrons indicates that a CI film exists on the steel pre-exposed in 2 M H<sub>2</sub>SO<sub>4</sub> solution + 5 mM 3ST. The observed N1s spectrum is decomposed into two peaks (399.5 and 401.4 eV). The first peak corresponds to the nitrogen atoms of the triazole group, while the second peak corresponds to the ammonium group of the substituent (Figure 10).

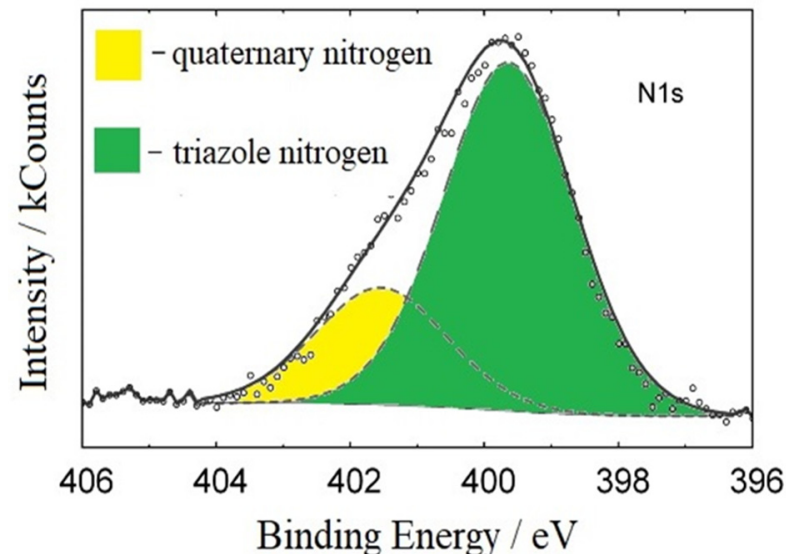


**Figure 10.** XPS spectrum of O1s electrons from the surface of carbon steel. Steel coupon processing: 2 M H<sub>2</sub>SO<sub>4</sub> + 5 mM 3ST, test duration—24 h.

Using the XPS MultiQuant program [46], the thicknesses of the layers formed on the surface were calculated taking into account the mean free path of electrons  $\lambda$ , determined by Campson and Seah formula [47]. The quantitative ratio of the XPS spectra of atoms on a steel surface exposed to the inhibited H<sub>2</sub>SO<sub>4</sub> solution without and with subsequent ultrasonic cleaning shows that a polymolecular CI layer thicker than 4 nm is formed on the metal. After ultrasonic cleaning of steel sample surfaces that removes the physically adsorbed inhibitor molecules, only a CI monolayer no thicker than 2 nm remains. The chemisorbed layer is strongly bound to the metal surface due to interaction with the surface iron atoms that form chemical bonds with the nitrogen atoms of the triazole ring. The XPS

spectrum of the steel surface contains no S2p-electron peak, which indicates that the film contains no sulfate anions. The surface of the metal under such a layer is oxidized to iron oxide when a sample is washed in the presence of air.

### 3.8. Protective Aftereffect of Thin 3ST Films

A qualitative confirmation that 3ST forms protective films on the surface of carbon steel in 2 M H<sub>2</sub>SO<sub>4</sub> solution is that the inhibitor manifests the so-called “protective aftereffect”. Indeed, the corrosion rate of steel samples exposed for 2–96 h to an inhibited solution (2 M H<sub>2</sub>SO<sub>4</sub> + 5 mM 3ST), then washed thoroughly and transferred to 2 M H<sub>2</sub>SO<sub>4</sub> background solution, is significantly lower than that of the metal without pretreatment in a solution containing the CI. The longer the coupon is pre-exposed in a solution containing 3ST, the lower the corrosion rate of steel is. After 48 h of exposure to the CI solution for inhibitor adsorption, the maximum corrosion slowdown by a factor of 13 was observed (Figure 11). The result obtained indicates that the protective layers formed by 3ST on steel have unique properties. Such layers are capable of protecting the metal in extremely corrosive acid solutions in the absence of an extra CI in the solution.

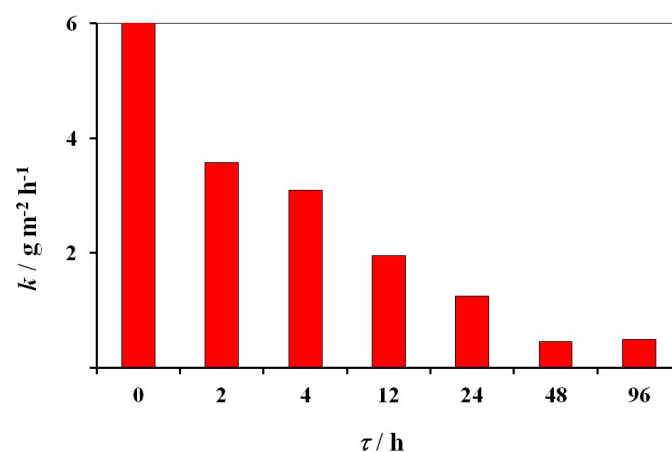


**Figure 11.** Plot of the steel corrosion rate in the background solution (2 M H<sub>2</sub>SO<sub>4</sub>, 2 h) vs. time ( $\tau$ , h) of preliminary exposure in 2 M H<sub>2</sub>SO<sub>4</sub> + 5 mM 3ST (2–96 h).

It was shown that 3ST is an effective inhibitor of corrosion and absorption of hydrogen by steel in sulfuric acid solutions. The observed effect is due to the formation of thin protective layers on the steel by the investigated corrosion inhibitor. Determination of the mechanism of action of this inhibitor is useful for the development of new acid corrosion inhibitors. The obtained results show that in order to effectively protect steel in a sulfuric acid solution, it is necessary to use compounds whose molecules form a protective layer on steels. The presented results are also important for the practice of using organic inhibitors to protect steels in sulfuric acid solutions. The investigated triazole can be introduced into industrial solutions of sulfuric acid to prevent corrosion of steel equipment in them. It is important that in this case the absorption of hydrogen by steel equipment is prevented.

## 4. Conclusions

1. Steel protection with the 3-substituted 1,2,4-triazole (3ST) in an H<sub>2</sub>SO<sub>4</sub> solution is accompanied by the formation of a polymolecular protective layer of CI molecules up to 4 nm thick on the metal. The lower 3ST monolayer that is adjacent to the metal is chemically bound to it. The overlying layers are bound to that layer and to each other by physical interaction. The efficiency of 3ST as an inhibitor of steel corrosion and hydrogen absorption by steel is determined by the specific features of its inhibitory action mechanism involving the formation of an organic protective layer on the metal surface. The formation of protective layers is confirmed by XPS and AFM data and by the results of studies on their protective aftereffects.

2. The rate constants of the main stages of hydrogen evolution and permeation into steel, both in the background H<sub>2</sub>SO<sub>4</sub> solution and in a solution containing 3ST, were calculated. It was shown that CI decreased the rate of the H<sup>+</sup> ion discharge reaction and the amount of hydrogen absorbed by steel.
3. Due to the reduction in the rate of hydrogen permeation into the metal by 3ST, the plastic properties of steel are partially preserved when it corrodes in H<sub>2</sub>SO<sub>4</sub> solutions, whereas complete loss of metal ductility occurs in the background environment.
4. Lastly, 3ST significantly slows down the anodic reaction of steel in H<sub>2</sub>SO<sub>4</sub> solution. This effect, along with the inhibition of the cathodic process, determines its efficiency as an inhibitor of steel corrosion in H<sub>2</sub>SO<sub>4</sub> solutions.

**Author Contributions:** Conceptualization: Y.G.A.; methodology: A.I.M.; formal analysis: T.A.N. and Y.G.A.; research: Y.G.A., A.Y.L. and T.A.N.; data processing: Y.G.A., T.A.N., A.I.M. and A.Y.L.; writing—preparation of the original project: Y.G.A.; writing—reviewing and editing: Y.G.A., A.I.M. and Y.I.K.; supervision: Y.I.K.; project administration: Y.I.K.; fundraising: Y.I.K. All authors have read and agreed to the published version of the manuscript.

**Funding:** The study was carried out within the framework of R&D (2022–2024): “Chemical resistance of materials, protection of metals and other materials from corrosion and oxidation” (registration number in EGISU 122011300078-1, No. FFZS-2022-0013).

**Institutional Review Board Statement:** Not applicable.

**Informed Consent Statement:** Informed consent was obtained from all subjects involved in the study.

**Data Availability Statement:** Data are unavailable due to privacy.

**Conflicts of Interest:** The authors declare no conflict of interest. The funders had no role in the design of the study; in the collection, analyses, or interpretation of data; in the writing of the manuscript; or in the decision to publish the results.

## References

1. Kuznetsov, Y.I.; Redkina, G.V. Thin Protective Coatings on Metals Formed by Organic Corrosion Inhibitors in Neutral Media. *Coatings* **2022**, *12*, 149. [[CrossRef](#)]
2. Shapagina, N.A.; Dushik, V.V. Application of Electrophoretic Deposition as an Advanced Technique of Inhibited Polymer Films Formation on Metals from Environmentally Safe Aqueous Solutions of Inhibited Formulations. *Materials* **2022**, *16*, 19. [[CrossRef](#)] [[PubMed](#)]
3. Petrunin, M.; Maksaeva, L.; Gladkikh, N.; Makarychev, Y.; Maleeva, M.; Yurasova, T.; Nazarov, A. Thin Benzotriazole Films for Inhibition of Carbon Steel Corrosion in Neutral Electrolytes. *Coatings* **2020**, *10*, 362. [[CrossRef](#)]
4. Gladkikh, N.; Petrunin, M.; Maksaeva, L.; Yurasova, T. Adsorption of Organosilanes on the Surface of Aluminium and the Formation of Organosilane Films to Protect It from Corrosion. *Materials* **2021**, *14*, 5757. [[CrossRef](#)] [[PubMed](#)]
5. Semiletov, A.M.; Chirkunov, A.A.; Grafov, O.Y.; Kuznetsov, Y.I. Stability of Superhydrophobic Layers Formed by Organic Acids on the Surface of Aluminum Alloy 6063. *Coatings* **2022**, *12*, 1468. [[CrossRef](#)]
6. Poling, G.W. Infrared Studies of Protective Films Formed by Acetylenic Corrosion Inhibitors. *J. Electrochem. Soc.* **1967**, *114*, 1209–1214. [[CrossRef](#)]
7. Barmatov, E.; La Terra, F.; Hughes, T. Mechanism of degradation of propargyl alcohol by acid-catalysed hydrolysis and corrosion inhibition efficiency of propargyl alcohol intermediates for carbon steel in hydrochloric acid. *Mater. Chem. Phys.* **2021**, *272*, 125048. [[CrossRef](#)]
8. Growcock, F.B.; Lopp, V.R. The inhibition of steel corrosion in hydrochloric acid with 3-phenyl-2-propyn-1-ol. *Corros. Sci.* **1988**, *28*, 397–410. [[CrossRef](#)]
9. Growcock, F.B.; Lopp, V.R.; Jasinski, R.J. Corrosion Protection of Oilfield Steel with 1-Phenyl-2-Propyn-1-ol. *J. Electrochem. Soc.* **1988**, *135*, 823–827. [[CrossRef](#)]
10. Bartos, M.; Kapusta, S.D.; Hackerman, N. A Study of Polymerization of Propargyl Alcohol on Steel. *J. Electrochem. Soc.* **1993**, *140*, 2604–2605. [[CrossRef](#)]
11. Aramaki, K.; Fujioka, E. Surface-Enhanced Raman Scattering Spectroscopy Studies on the Inhibition Mechanism of Propargyl Alcohol for Iron Corrosion in Hydrochloric Acid. *Corrosion* **1996**, *52*, 83–91. [[CrossRef](#)]
12. Frignani, A.; Monticelli, C.; Zucchi, F.; Trabanelli, G. Acetylenic alcohols as inhibitors of iron acid corrosion. Improvement of the inhibition efficiency of a class of substances based on their action mechanism. *Int. J. Corros. Scale Inhib.* **2014**, *3*, 105–119. [[CrossRef](#)]

13. Aramaki, K.; Fujioka, E. Spectroscopic investigations on the inhibition mechanism of propargyl alcohol for iron corrosion in hydrochloric acid at elevated temperatures. *Corrosion* **1997**, *53*, 319–326. [[CrossRef](#)]
14. Growcock, F.B.; Lopp, V.R. Film Formation on Steel in Cinnamaldehyde-Inhibited Hydrochloric Acid. *Corrosion* **1988**, *44*, 248–254. [[CrossRef](#)]
15. Gao, J.; Weng, Y.; Salitanate; Li, F.; Hong, Y. Corrosion inhibition of  $\alpha,\beta$ -unsaturated carbonyl compounds on steel in acid medium. *Pet. Sci.* **2009**, *6*, 201–207. [[CrossRef](#)]
16. Kumar, D.; Muralidhar, V.K.; Jain, V.; Rai, B. Integrating experiments, DFT and characterization for comprehensive corrosion inhibition studies—A case for cinnamaldehyde as an excellent green inhibitor for steels in acidic media. *Corros. Sci.* **2022**, *208*, 110623. [[CrossRef](#)]
17. Avdeev, Y.G.; Kuznetsov, Y.I.; Buryak, A.K. Inhibition of steel corrosion by unsaturated aldehydes in solutions of mineral acids. *Corros. Sci.* **2013**, *69*, 50–60. [[CrossRef](#)]
18. Avdeev, Y.G.; Kuznetsov, Y.I. Inhibitor protection of steel corrosion in acid solutions at high temperatures. A review. Part 2. *Int. J. Corros. Scale Inhib.* **2020**, *9*, 867–902. [[CrossRef](#)]
19. Obot, I.B.; Meroufel, A.; Onyeachu, I.B.; Alenazi, A.; Sorour, A.A. Corrosion inhibitors for acid cleaning of desalination heat exchangers: Progress, challenges and future perspectives. *J. Mol. Liq.* **2019**, *296*, 111760. [[CrossRef](#)]
20. Verma, C.; Quraishi, M.A.; Ebenso, E.E. Corrosive electrolytes. *Int. J. Corros. Scale Inhib.* **2020**, *9*, 1261–1276. [[CrossRef](#)]
21. Avdeev, Y.G.; Gorichev, I.G.; Luchkin, A.Y. Effect of IFKhan-92 inhibitor on scale removal during sulfuric acid pickling of steel. *Int. J. Corros. Scale Inhib.* **2012**, *1*, 26–37. [[CrossRef](#)]
22. Schmitt, G. Application of Inhibitors for Acid Media: Report prepared for the European Federation of Corrosion Working Party on Inhibitors. *Br. Corros. J.* **1984**, *19*, 165–176. [[CrossRef](#)]
23. Pradhan, A.; Vishwakarma, M.; Dwivedi, S.K. A review: The impact of hydrogen embrittlement on the fatigue strength of high strength steel. *Mater. Today: Proceed.* **2020**, *26*, 3015–3019. [[CrossRef](#)]
24. Ohaeri, E.; Eduok, U.; Szpunar, J. Hydrogen related degradation in pipeline steel: A review. *Int. J. Hydrog. Energy* **2018**, *43*, 14584–14617. [[CrossRef](#)]
25. Liu, Q.; Zhou, Q.; Venezuela, J.; Zhang, M.; Wang, J.; Atrens, A. A review of the influence of hydrogen on the mechanical properties of DP, TRIP, and TWIP advanced high-strength steels for auto construction. *Corros. Rev.* **2016**, *34*, 127–152. [[CrossRef](#)]
26. Lunarska, E.; Nikiforov, K. Hydrogen Degradation of the Refinery and Electric Power Installations. *Corros. Rev.* **2008**, *26*, 173–213. [[CrossRef](#)]
27. Ramamurthy, S.; Atrens, A. Stress corrosion cracking of high-strength steels. *Corros. Rev.* **2013**, *31*, 1–31. [[CrossRef](#)]
28. Avdeev, Y.G.; Nenasheva, T.A.; Luchkin, A.Y.; Marshakov, A.I.; Kuznetsov, Y.I. Effect of Quaternary Ammonium Salts and 1,2,4-Triazole Derivatives on Hydrogen Absorption by Mild Steel in Hydrochloric Acid Solution. *Materials* **2022**, *15*, 6989. [[CrossRef](#)]
29. Muralidharan, S.; Quraishi, M.A.; Iyer, S.V.K. The effect of molecular structure on hydrogen permeation and the corrosion inhibition of mild steel in acidic solutions. *Corros. Sci.* **1995**, *37*, 1739–1750. [[CrossRef](#)]
30. Hari Kumar, S.; Vivekanand, P.A.; Kamaraj, P. The inhibitive effect of cloxacillin on mild steel corrosion in 2 N Sulphuric acid medium. *Mater. Today Proc.* **2021**, *36*, 898–902. [[CrossRef](#)]
31. Ansari, K.R.; Chauhan, D.S.; Singh, A.; Saji, V.S.; Quraishi, M.A. Corrosion inhibitors for acidizing process in oil and gas sectors. In *Corrosion Inhibitors in the Oil and Gas Industry*; Saji, V.S., Umoren, S.A., Eds.; Wiley-VCH Verlag GmbH & Co. KGaA: Weinheim, Germany, 2020; pp. 153–176. [[CrossRef](#)]
32. Quraishi, M.A.; Chauhan, D.S.; Saji, V.S. Heterocyclic corrosion inhibitors for acid environments. In *Heterocyclic Organic Corrosion Inhibitors*; Quraishi, M.A., Chauhan, D.S., Saji, V.S., Eds.; Elsevier Inc.: Amsterdam, The Netherlands, 2020; pp. 87–131. [[CrossRef](#)]
33. Phadke Swathi, N.; Alva, V.D.P.; Samshuddin, S. A Review on 1,2,4-Triazole Derivatives as Corrosion Inhibitors. *J. Bio-Tribo-Corros.* **2017**, *3*, 42. [[CrossRef](#)]
34. Avdeev, Y.G.; Kuznetsov, Y.I. Nitrogen-containing five-membered heterocyclic compounds as corrosion inhibitors for metals in solutions of mineral acids—An overview. *Int. J. Corros. Scale Inhib.* **2021**, *10*, 480–540. [[CrossRef](#)]
35. Devanathan, M.A.V.; Stachurski, Z. The adsorption and diffusion of electrolytic hydrogen in palladium. *Proceed. R. Society. Ser. A Math. Phys. Sci.* **1962**, *270A*, 90–540. [[CrossRef](#)]
36. Devanathan, M.A.V.; Stachurski, Z. The Mechanism of Hydrogen Evolution on Iron in Acid Solutions by Determination of Permeation Rates. *J. Electrochem. Soc.* **1964**, *111*, 619–623. [[CrossRef](#)]
37. Wagner, C.D.; Davis, L.E.; Zeller, M.V.; Taylor, J.A.; Raymond, R.H.; Gale, L.H. Empirical atomic sensitivity factors for quantitative analysis by electron spectroscopy for chemical analysis. *Surf. Interf. Anal.* **1981**, *3*, 211–225. [[CrossRef](#)]
38. Shirley, D.A. High-Resolution X-Ray Photoemission Spectrum of the Valence Bands of Gold. *Phys. Rev. B* **1972**, *5*, 4709–4714. [[CrossRef](#)]
39. Avdeev, Y.G.; Kuznetsov, D.S.; Makarychev, Y.B.; Kazansky, L.P. Protective Aftereffect of IFKhan-92 Inhibitor for Corrosion of Nickel–Chromium Steel in Hydrochloric Acid. *Prot. Met. Phys. Chem. Surf.* **2020**, *56*, 1264–1269. [[CrossRef](#)]
40. Iyer, R.N.; Pickering, H.W.; Zamanzadeh, M. Analysis of hydrogen evolution and entry into metals for the discharge-recombination process. *J. Electrochem. Soc.* **1989**, *136*, 2463–2470. [[CrossRef](#)]
41. Popov, B.N.; Lee, J.-W.; Djukic, M.B. Chapter 7. Hydrogen permeation and hydrogen-induced cracking. In *Handbook of Environmental Degradation of Materials*, 3rd ed.; Kutz, M., Ed.; Elsevier Inc.: Amsterdam, The Netherlands, 2018; pp. 133–162. [[CrossRef](#)]

42. Damaskin, B.B.; Afanas'ev, B.N. Current state of the theory of the effect of the adsorption of organic substances on the kinetics of electrochemical reactions. *Sov. Elektrokimiya* **1977**, *13*, 1099–1117. (In Russian)
43. Marshakov, A.I.; Nenasheva, T.A. Effect of sorbed hydrogen on iron dissolution in the presence of tetraethylammonium cations. *Prot. Met. Phys. Chem. Surf.* **2002**, *38*, 556–562. [[CrossRef](#)]
44. Afanas'ev, B.N.; Skobochkina, Y.P.; Serdyukova, G.G. *Physicochemical Bases of the Action of Corrosion Inhibitors*; Publishing House of UdGu: Moscow, Russia, 1990; p. 20. (In Russian)
45. Kiuchi, K.; McLellan, R.B. The solubility and diffusivity of hydrogen in well-annealed and deformed iron. *Acta Metall.* **1983**, *31*, 961–984. [[CrossRef](#)]
46. Mohai, M. XPS Multi Quant: Multimodel XPS quantification software. *Surf. Interface Anal.* **2004**, *36*, 828–832. [[CrossRef](#)]
47. Cumpson, P.J.; Seah, M.P. Elastic Scattering Corrections in AES and XPS. II. Estimating Attenuation Lengths and Conditions Required for their Valid Use in Overlay/Substrate Experiments. *Surf. Interface Anal.* **1997**, *25*, 430–446. [[CrossRef](#)]

**Disclaimer/Publisher's Note:** The statements, opinions and data contained in all publications are solely those of the individual author(s) and contributor(s) and not of MDPI and/or the editor(s). MDPI and/or the editor(s) disclaim responsibility for any injury to people or property resulting from any ideas, methods, instructions or products referred to in the content.